

# ChemComm

Accepted Manuscript



This is an *Accepted Manuscript*, which has been through the Royal Society of Chemistry peer review process and has been accepted for publication.

*Accepted Manuscripts* are published online shortly after acceptance, before technical editing, formatting and proof reading. Using this free service, authors can make their results available to the community, in citable form, before we publish the edited article. We will replace this *Accepted Manuscript* with the edited and formatted *Advance Article* as soon as it is available.

You can find more information about *Accepted Manuscripts* in the [Information for Authors](#).

Please note that technical editing may introduce minor changes to the text and/or graphics, which may alter content. The journal's standard [Terms & Conditions](#) and the [Ethical guidelines](#) still apply. In no event shall the Royal Society of Chemistry be held responsible for any errors or omissions in this *Accepted Manuscript* or any consequences arising from the use of any information it contains.

Cite this: DOI: 10.1039/c0xx00000x

www.rsc.org/xxxxxx

ARTICLE TYPE

# High-performance Supercapacitor Electrodes based on hierarchical Ti@MnO<sub>2</sub> Nanowire Arrays

Dongdong Zhu,<sup>1,2</sup> Yadong Wang<sup>3</sup>, Guoliang Yuan<sup>1</sup> and Hui Xia,<sup>1,2,\*</sup>

Received (in XXX, XXX) Xth XXXXXXXXXX 20XX, Accepted Xth XXXXXXXXXX 20XX

DOI: 10.1039/b000000x

Ti nanowire arrays (NAs) prepared by a facile and template-free hydrothermal method were used as three-dimensional (3D) current collector for the electrodeposition of MnO<sub>2</sub>. The resulting Ti@MnO<sub>2</sub> NAs exhibit remarkable electrochemical behavior with high specific capacitance, good rate performance and desirable cycling stability.

Recently, supercapacitors (SCs) have attracted extensive research interests because of their intrinsic characteristics such as high power density, fast charge-discharge rate, long service life and low maintenance cost. These outstanding advantages make SCs very promising candidates for applications in numerous fields, including portable electronic devices, backup power sources, electric vehicles and renewable energy power plants.<sup>1-5</sup> However, the major bottleneck of commercial SCs based on carbonaceous materials is their low energy density. Therefore, it is imperative to develop new electrode materials with both high energy and high power densities. Among various electrode materials, transition metal oxides are the most attractive candidates due to their high energy density arising from the fast and reversible faradaic redox reactions at the electrode/electrolyte interfaces.<sup>6-10</sup>

Compared to other transition metal oxides, MnO<sub>2</sub> was the most investigated material because of its intriguing features including natural abundance, low cost, environmental benignity and high theoretical specific capacitance (1370 F g<sup>-1</sup>). However, limited by the poor electrical conductivity and limited surface area, the theoretical specific capacitance has rarely been achieved in bulk MnO<sub>2</sub>.<sup>11-15</sup> Two effective strategies were often used to improve the supercapacitive performance of MnO<sub>2</sub>: making nanosized MnO<sub>2</sub> to increase the surface area and incorporating conductive additives to improve the electrical conductivity. Recently, great progress have been made by depositing MnO<sub>2</sub> nanoparticles on conductive metal oxide NAs, such as SnO<sub>2</sub> and Zn<sub>2</sub>SnO<sub>4</sub>, which were used as 3D current collectors to improve the electrical conductivity and capacitive performance.<sup>8,16-21</sup> The enhanced electrochemical performance can be attributed to the large surface areas, short ion diffusion pathways and relatively good electrical conductivity. Usually, the electrical conductivity of metal oxides is far below that of metals. However, very limited papers have been reported for using metal NAs as 3D current collectors for depositing MnO<sub>2</sub> nanoparticles as electrodes for supercapacitors, which are probably due to the lacking of facile methods to fabricate metal NAs. The mostly used method to fabricate metal NAs is the template-assisted method, which includes complex

experimental procedures and is not suitable for large-scale fabrication.<sup>22-24</sup>

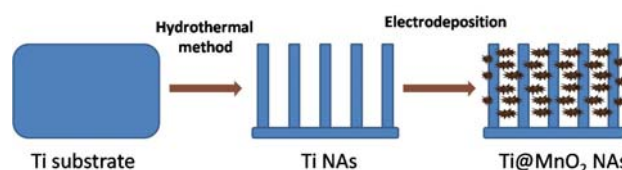


Fig. 1 Schematic illustration of the fabrication process of the Ti@MnO<sub>2</sub> NAs.

Herein, we developed a simple method to prepare hierarchical Ti@MnO<sub>2</sub> NAs for high-performance supercapacitors (see details in ESI†). The fabrication procedure is schematically illustrated in Fig. 1. Ti can be dissolved in HCl solution under certain condition.<sup>25</sup> In this work, Ti NAs were formed on the Ti substrate by a etching process in an appropriate concentration of HCl solution under hydrothermal treatment. It is speculated that the preformed TiO<sub>2</sub> layer on the Ti substrate is not uniform, inducing different etching rates at the surface of Ti substrate. The different etching rates at the surface probably result in a relatively selective etching, thus forming the nanowire structure of Ti. It is also possible that the etching is relatively anisotropic, tending to form the nanowires on the Ti substrate.

Fig. 2a shows the scanning electron microscopy (SEM) image of a planar Ti foil, revealing a flat surface with some cavities. After the hydrothermal treatment with acid solution, freestanding and homogeneously aligned Ti NAs were formed on the substrate (Fig. 2b). The morphology of Ti NAs was greatly influenced by the hydrothermal conditions (Fig. S1, ESI†). In the present study, a hydrothermal reaction at 180°C for 16 h can lead to the best morphology. The Ti nanowires are rectangular in shape with diameters ranging between 10 and 50 nm. Fig. 2c shows the SEM image of the MnO<sub>2</sub> thin film directly electrodeposited on the Ti foil. The film is highly porous and comprised of thin MnO<sub>2</sub> nanoflakes. Fig. 2d shows the SEM image of the Ti@MnO<sub>2</sub> NAs. Obviously, amorphous MnO<sub>2</sub> nanoflakes (as confirmed by the XRD in Fig. S2, ESI†) are uniformly covered on the surface of Ti NAs and fill the space in between (Fig. S3, ESI†). A cross-section transmission electron microscopy (TEM) specimen of the Ti@MnO<sub>2</sub> NAs was prepared by a focused ion beam (FIB) system. As show in Fig. 2e, a clear interface between Ti@MnO<sub>2</sub> NAs and Ti substrate can be observed. The NAs are randomly orientated on the Ti substrate with an average length of about 300

nm. As shown in the high-magnification TEM image (Fig. S4, ESI<sup>†</sup>), MnO<sub>2</sub> was found deposited on the Ti NWs even at the bottom interface area. The Pt nanoparticles filled in the space between Ti@MnO<sub>2</sub> NWs were deposited during the FIB milling process for sample protection (Fig. S4, ESI<sup>†</sup>). Elemental mapping by energy-dispersive X-ray spectroscopy (EDS) further confirmed the Ti NAs/Ti substrate interface and the successful deposition of MnO<sub>2</sub> onto the surface of Ti NAs, agreeing well with the SEM results.

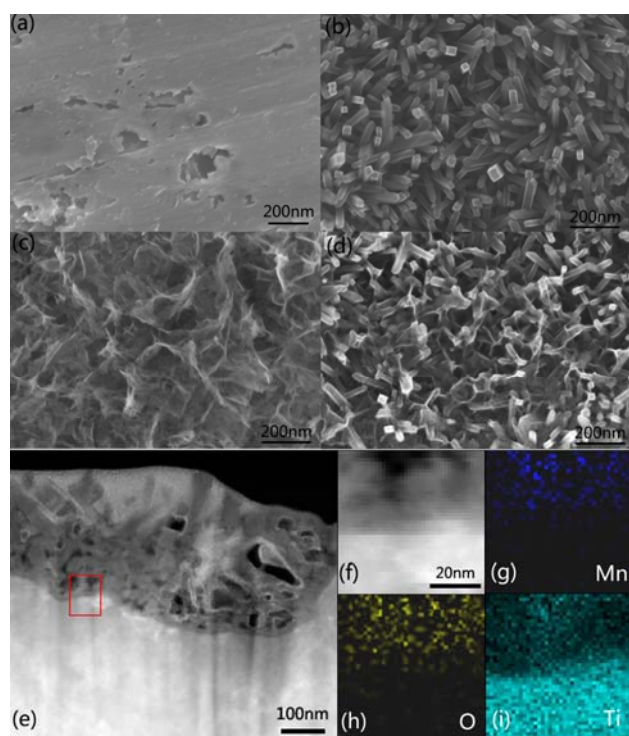


Fig. 2 SEM images of (a) Ti substrate, (b) Ti NAs, (c) MnO<sub>2</sub> film and (d) Ti@MnO<sub>2</sub> NAs, (e) cross-section TEM image of Ti@MnO<sub>2</sub> NAs, (f) enlarged TEM and EDS element maps of (g) Mn, (h) O and (i) Ti for the red square area in (e).

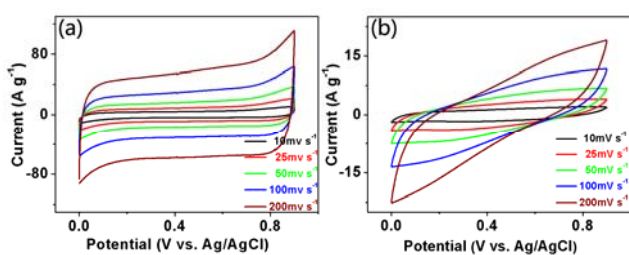


Fig. 3 CV curves of (a) the Ti@MnO<sub>2</sub> NAs and (b) the MnO<sub>2</sub> thin film at different scan rates.

Fig. 3 shows the cyclic voltammetry (CV) curves of the Ti@MnO<sub>2</sub> NAs and the MnO<sub>2</sub> thin film between 0 and 0.9 V vs. Ag/AgCl at different scan rates ranging from 10 to 200 mV s<sup>-1</sup> in 1M Na<sub>2</sub>SO<sub>4</sub> aqueous electrolyte. As shown in Fig. 3a, the CV curves of the Ti@MnO<sub>2</sub> NAs exhibit quasi-rectangular shape with a mirror image feature at all scan rates, which indicates the ideal capacitive behavior and high rate capability for the Ti@MnO<sub>2</sub> NAs. In contrast, the CV curves of the MnO<sub>2</sub> thin film were severely distorted, especially at high scan rates, with much smaller enclosed areas (Fig. 3b). Thus, by electrodepositing

MnO<sub>2</sub> thin film on the Ti NAs, rather than the planar Ti substrate, larger specific capacitance and greatly enhanced rate performance can be achieved.

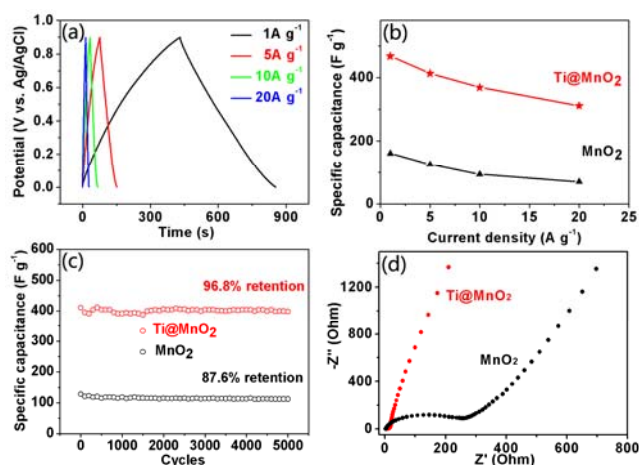


Fig. 4 (a) GCD curves of the Ti@MnO<sub>2</sub> NAs at different current densities, (b) specific capacitance of the Ti@MnO<sub>2</sub> NAs and the MnO<sub>2</sub> thin film at different current densities, (c) cycling performance of the Ti@MnO<sub>2</sub> NAs and the MnO<sub>2</sub> thin film at a current density of 5 A g<sup>-1</sup>, (d) Nyquist plots of the Ti@MnO<sub>2</sub> NAs and the MnO<sub>2</sub> thin film.

The galvanostatic charge-discharge (GCD) curves of the Ti@MnO<sub>2</sub> NAs at different current densities are shown in Fig. 4a. The symmetric GCD curves with fairly linear slopes apparently demonstrate good electrochemical capacitive characteristics and superior reversibility of the Ti@MnO<sub>2</sub> NAs. No obvious internal resistance drop is observed at the beginning of the discharge curve, indicating a low internal resistance for the Ti@MnO<sub>2</sub> NAs. Fig. 4b shows the specific capacitances of the Ti@MnO<sub>2</sub> NAs and the MnO<sub>2</sub> thin film calculated from the GCD curves at different current densities. Impressively, the Ti@MnO<sub>2</sub> NAs can deliver much higher specific capacitances of 467.8, 413.3, 369.3 and 311.5 F g<sup>-1</sup> at current densities of 1, 5, 10 and 20 A g<sup>-1</sup>, respectively, compared to 160.5, 125.8, 94.1 and 70.4 F g<sup>-1</sup> for the MnO<sub>2</sub> thin film. In addition, when the current density increased from 1 to 20 A g<sup>-1</sup>, about 66.5% of specific capacitance was retained for the Ti@MnO<sub>2</sub> NAs. In contrast, only 43.9% retention was retained for the MnO<sub>2</sub> film, indicating superior rate capability of the Ti@MnO<sub>2</sub> NAs.

Cycling stability is another critical factor that determines the practical applications of SCs. The cycling performance of the Ti@MnO<sub>2</sub> NAs and the MnO<sub>2</sub> thin film was investigated by GCD cycling at a current density of 5 A g<sup>-1</sup> for 5000 cycles. As shown in Fig. 4c, the specific capacitance of the Ti@MnO<sub>2</sub> NAs fluctuated slightly for the initial 1500 cycles and then was relatively constant. After 5000 cycles, the specific capacitance retention for the Ti@MnO<sub>2</sub> NAs was 96.8%, while it was only 87.6% for the MnO<sub>2</sub> thin film, illustrating the excellent long-term cyclability of the Ti@MnO<sub>2</sub> NAs.

The electrochemical impedance spectra (EIS) of the Ti@MnO<sub>2</sub> NAs and the MnO<sub>2</sub> thin film electrodes were measured to understand their different electrochemical behaviors. EIS measurements were performed over the frequency range from 0.01 to 10<sup>5</sup> Hz under open-circuit potential, and the

corresponding Nyquist plots are shown in Fig.4d. The Nyquist plots of both the Ti@MnO<sub>2</sub> NAs and the MnO<sub>2</sub> thin film electrodes exhibit a straight line in the low frequency region, a depressed semicircle in the high-to-medium frequency region, and a high frequency intercept in the real Z' axis. At high frequencies, the almost same intercepts for both the Ti@MnO<sub>2</sub> NAs and the MnO<sub>2</sub> thin film electrodes indicate the two electrodes have similar overall ohmic resistance. However, compared with the MnO<sub>2</sub> thin film, the diameter of the semicircle for the Ti@MnO<sub>2</sub> NAs is much smaller, revealing a greatly reduced charge-transfer resistance ( $R_{ct}$ ). The reduced  $R_{ct}$  should be attributed to the large surface area and remarkably improved electrical conductivity of the Ti@MnO<sub>2</sub> NAs. In the low frequency regime, the EIS spectrum of the Ti@MnO<sub>2</sub> NAs exhibits a more vertical straight line along the imaginary axis, indicating a lower diffusion resistance.

The superior electrochemical performance of the Ti@MnO<sub>2</sub> NAs can be attributed to its hierarchical architecture and synergetic effect between Ti NAs and MnO<sub>2</sub> nanoflakes. First, the Ti NAs can function as 3D current collector, providing electron "superhighway" for effective charge storage and delivery. Second, comparing with 2D Ti foil, the 3D Ti NAs provide a much larger surface area for the deposition of MnO<sub>2</sub> nanoflakes, leading to more electroactive sites for the charge storage. Third, the ultrathin amorphous MnO<sub>2</sub> nanoflakes enable fast and reversible faradic reaction by providing short ion diffusion paths, and the highly porous and open structure of Ti@MnO<sub>2</sub> NAs benefits the penetration of electrolyte. Last but not the least, since the Ti NAs were fabricated by directly etching of the Ti foil, they have excellent mechanical adhesion and electrical connection to the substrate, enabling each MnO<sub>2</sub> nanoflake effectively participates in the redox reaction without "dead" volume. Due to the facile preparation method for Ti NAs, future works could be extended to prepare Ti@Co<sub>3</sub>O<sub>4</sub>, Ti@SnO<sub>2</sub>, and etc. as 3D electrodes for both supercapacitors and thin film microbatteries.

## Conclusions

In summary, Ti NAs synthesized by a facile, template-free hydrothermal method were for the first time used as 3D scaffolds to fabricate hierarchical Ti@MnO<sub>2</sub> NAs. The freestanding Ti nanowires provided large surface area for the deposition of MnO<sub>2</sub> nanoflakes, enabling a high utilization of MnO<sub>2</sub>. More importantly, compared with previous reported metal oxides NAs, the Ti NAs can serve as high electronic conducting framework for enhancing the rate capability of MnO<sub>2</sub>-based electrode. The smartly designed Ti@MnO<sub>2</sub> NAs exhibited outstanding electrochemical performance, in terms of large specific capacitance (467.8 F g<sup>-1</sup> at 1 A g<sup>-1</sup>), desirable rate capability (66.5% capacitive retention at a high current density of 20 A g<sup>-1</sup>) and remarkable cycling stability (only 3.2% capacitance degradation after 5000 cycles). These results indicate that the hierarchical Ti@MnO<sub>2</sub> NAs have great potential as electrode for the next generation high-performance supercapacitors. Moreover, the Ti NAs can open up new opportunities for the application in considerable fields such as Li-ion battery, photocatalysis, biosensor, and etc.

This work was supported by National Natural Science

Foundation of China (No. 51102134 and 11134004), Natural Science Foundation of Jiangsu Province (No. BK20131349), China Postdoctoral Science Foundation (No. 2013M530258), and Jiangsu Planned Projects for Postdoctoral Research Funds (No. 1202001B).

## Notes and references

- <sup>1</sup> *School of Materials Science and Engineering, Nanjing University of Science and Technology, Xiaolingwei 200, Nanjing 210094, China. Fax: XX XXXX XXXX; Tel: XX XXXX XXXX; E-mail: xiahui@njjust.edu.cn*
- <sup>2</sup> *Herbert Gleiter Institute of Nanoscience, Nanjing University of Science and Technology, Xiaolingwei 200, Nanjing 210094, China*
- <sup>3</sup> *School of Engineering, Nanyang Polytechnic, 180 Ang Mo Kio Ave 8, Singapore 569830*
- † Electronic Supplementary Information (ESI) available: [Experimental details, SEM images of Ti NAs prepared at different hydrothermal conditions, enlarged SEM and TEM images of the Ti@MnO<sub>2</sub> NAs]. See DOI: 10.1039/b000000x/
- ‡ Footnotes should appear here. These might include comments relevant to but not central to the matter under discussion, limited experimental and spectral data, and crystallographic data.
- 1 G. P. Wang, L. Zhang and J. J. Zhang, *Chem. Soc. Rev.*, 2012, 41, 797.
- 2 C. Z. Yuan, L. Yang, L. R. Hou, L. F. Shen, X. G. Zhang and X. W. Lou, *Energy Environ. Sci.*, 2012, 5, 7883.
- 3 Q. T. Qu, Y. S. Zhu, X. W. Gao and Y. P. Wu, *Adv. Energy Mater.*, 2012, 2, 950.
- 4 H. C. Chen, J. J. Jiang, L. Zhang, H. Z. Wan, T. Qi and D. D. Xia, *Nanoscale*, 2013, 5, 8879.
- 5 L. F. Chen, Z. H. Huang, H. W. Liang, Q. F. Guan and S. H. Yu, *Adv. Mater.*, 2013, 25, 4746.
- 6 Z. N. Yu, B. Duong, D. Abbitt and J. Thomas, *Adv. Mater.*, 2013, 25, 3302.
- 7 P. H. Yang, X. Xiao, Y. Z. Li, Y. Ding, P. F. Qiang, X. H. Tan, W. J. Mai, Z. Y. Lin, W. Z. Wu, T. Q. Li, H. Y. Jin, P. Y. Liu, J. Zhou, C. P. Wang and Z. L. Wang, *ACS Nano*, 2013, 7, 2617.
- 8 L. Yu, G. Q. Zhang, C. Z. Yuan and X. W. Lou, *Chem. Commun.*, 2013, 49, 137.
- 9 X. M. Feng, Z. Z. Yan, N. N. Chen, Y. Zhang, Y. W. Ma, X. F. Liu, Q. L. Fan, L. H. Wang and W. Huang, *J. Mater. Chem. A*, 2013, 1, 12818.
- 10 X. H. Lu, G. M. Wang, T. Zhai, M. H. Yu, J. Y. Gan, Y. X. Tong and Y. Li, *Nano Lett.*, 2012, 12, 1690.
- 11 H. Jiang, C. Z. Li, T. Sun and J. Ma, *Chem. Commun.*, 2012, 48, 2606.
- 12 Z. P. Sun, S. Firdoz, E. Y. Yap, L. Li and X. M. Lu, *Nanoscale*, 2013, 5, 4379.
- 13 J. C. Chou, Y. L. Chen, M. H. Yang, Y. Z. Chen, C. C. Lai, H. T. Chiu, C. Y. Lee, Y. L. Chueh and J. Y. Gan, *J. Mater. Chem. A*, 2013, 1, 8753.
- 14 J. Y. Tao, N. S. Liu, W. Z. Ma, L. W. Ding, L. Y. Li, J. Su and Y. H. Gao, *Sci. Rep.*, 2013, 3, 2286.
- 15 H. Pang, S. M. Wang, G. C. Li, Y. H. Ma, J. Li, X. X. Li, L. Zhang, J. S. Zhang and H. H. Zheng, *J. Mater. Chem. A*, 2013, 1, 5053.
- 16 X. Sun, Q. Li, Y. N. Lü and Y. B. Mao, *Chem. Commun.*, 2013, 49, 4456.
- 17 J. P. Liu, J. Jiang, C. W. Cheng, H. X. Li, J. X. Zhang, H. Gong and H. J. Fan, *Adv. Mater.*, 2011, 23, 2076.
- 18 J. Yan, E. Khoo, A. Sumboja and P. S. Lee, *ACS Nano*, 2010, 4, 4247.
- 19 J. Jiang, Y. Y. Li, J. P. Liu, X. T. Huang, C. Z. Yuan and X. W. Lou, *Adv. Mater.*, 2012, 24, 5166.
- 20 X. H. Lu, T. Zhai, X. H. Zhang, Y. Q. Shen, L. Y. Yuan, B. Hu, L. Gong, J. Chen, Y. H. Gao, J. Zhou, Y. X. Tong and Z. L. Wang, *Adv. Mater.*, 2012, 24, 938.
- 21 J. X. Li, M. Yang, J. P. Wei and Z. Zhou, *Nanoscale*, 2012, 4, 4498.
- 22 Y. Lei, B. Daffos, P. L. Taberna, P. Simon and F. Favier, *Electrochim. Acta.*, 2010, 55, 7454.
- 23 W. B. Yan, J. Y. Kim, W. D. Xing, K. C. Donovan, T. Ayyvazian and R. M. Penner, *Chem. Mater.*, 2012, 24, 2382.
- 24 Y. L. Chen, P. C. Chen, T. L. Chen, C. Y. Lee and H. T. Chiu, *J. Mater. Chem. A*, 2013, 1, 13301.
- 25 N. K. Allam and C. A. Grimes, *J. Phys. Chem. C*, 2007, 111, 13028.